Supporting Information for:

Alteration of Sediments by Hyperalkaline K-Rich Cement Leachate: Implications for Strontium Adsorption and Incorporation.

Sarah H. Wallace[1], Samuel Shaw[1,2], Katherine Morris[2], Joe S. Small[3] and Ian T. Burke[1]*

[1] Earth Surface Science Institute, School of Earth and Environment, University of Leeds, Leeds, LS2 9JT, UK. *Corresponding Author's E-mail: I.T.Burke@leeds.ac.uk; Phone: +44 113 3437532; Fax: +44 113 3435259

[2] Research Centre for Radwaste and Decommissioning and Williamson Research Centre, School of Earth, Atmospheric and Environmental Sciences, The University of Manchester, Manchester, M13 9PL, U.K.

[3] National Nuclear Laboratory, Risley, Warrington, Cheshire, WA3 6AE, U.K.

This section consists of 11 pages, 5 tables and 2 figures.

Prepared for Environmental Science and Technology, 20 March 2013

Section S1: Detailed Solid Analysis Methods

Electron Microscopy Selected sediment samples were prepared for SEM analysis on a FEI QUANTA 650 Field Emission Gun Environmental Scanning Electron Microscope (accelerating voltage = 10 kV, working distance = 13.6 mm) by washing twice with deionised water, followed by a final wash with ethanol. Sediments were dried and then mounted onto 10 mm aluminium stubs and carbon coated to 10 nm. Energy dispersive X-ray microanalysis (EDX) was performed on selected ~ 10 µm spots using an Oxford Instruments INCA 250 system (count time of 90 secs). Additional samples of the 365 days +70°C sediment were prepared for analysis by electron microprobe on a JEOL JXA 8230 Superprobe. Washed sediment was set in a 30 mm resin epoxy block, polished and carbon coated to 10 nm. Beam conditions were 15kV, 10nA current and 6µm beam diameter. Count times for peak/background (in seconds) were: Sr and Ba, 60 s / 30 s; Si and Al, 20 s /10 s; Fe, 30 s /15 s; all other elements, 10 s /5 s. The following standards were used for elemental calibration: Diopside ($CaMgSi_2O_6$) for Si, Ca and Mg; Hematite (Fe_2O_3) for Fe; K-feldspar ($KAlSi_3O_8$) for K; Jadeite ($NaAlSi_2O_6$) for Na; Barite ($BaSO_4$) for Ba; Celestine ($SrSO_4$) for Sr and Kyanite (Al_2SiO_5) for Al.

X-ray Diffraction (XRD) Diffraction patterns were collected from fine fraction samples (separated by suspension in methanol) of selected reacted sediments. To separate the fine fraction approximately 0.5 g bulk sediment sample was suspended in 5 ml methanol and sonicated for 15 minutes in an ultrasonic bath, after which time the suspension was allowed to settle for 10 minutes. The supernatant was then withdrawn and microcentrifuged at 6000 g to collect the fine fraction. After separation, the samples were washed twice with deionised water and once with ethanol, before being air dried and ground in a pestle and mortar. Samples were analysed over 5 to 70 ° 2θ with step size of 0.01 and 155 seconds/step on a Bruker D8 Advance XRD with Cu K-alpha radiation. Identification of phases in XRD traces was achieved using peak match software the DIFFRAC.SUITE software (Bruker).

BET Surface Area The BET surface area (SSA_{BET}) of sediments reacted for 10, 30, 90, 180 and 365 days and 365 days + 70 °C was measured by degassing with N_2 on a Micromeritics FlowPrep 060 sample degas system prior to analysis with a Micromeritics Gemini V BET surface area analyser. The samples were degassed for 19hours at 21C, following the procedure of [1]. This procedure ensures an accurate BET surface area analysis without any phase alteration which can be caused by heating.

Table S1. Sequential extraction scheme based on [2], adapted for use with anoxic samples [3, 4] and for use with Sr-90 radiolabeled sediments[5].

Fraction	Target Phase	Leachate Composition	Leach Time
Porewater	Soluble Sr^{2+}	Supernatant	
Exchangeable	Weakly sorbed exchangeable Sr	1 mol L^{-1} magnesium chloride (pH 7)	2 hours
Carbonate	Sr adsorbed or bound to carbonates	1 mol L^{-1} sodium acetate, adjusted to pH 5 with acetic acid	5 hours
Acid extractable / reducible	Sr bound to Fe-Mn-oxyhydroxides and zeolites	(0.5 mol L^{-1}) hydroxylammonium chloride, adjusted to pH1.5 with HCl	12 hours
Residual	Sr held within the mineral matrix	Sr-90 activity not removed during previous steps	

Section S2: Detailed Water Sampling and Scintillation Counting Methods

At each sampling point, 1 ml of the supernatant removed from experiments was used to determine total ^{90}Sr + ^{90}Y activity by liquid scintillation counting (1 ml sample per 10 ml EcoscintA scintillation cocktail, National Diagnostics USA; count time, 10 minutes; energy window, 30-1020 keV) on a Parkard Tri-Carb 2100TR Liquid Scintillation Analyzer. Samples were decay stored for a minimum of 35 days prior to counting to allow for secular equilibrium with ^{90}Y to be attained, and for any unsupported aqueous ^{90}Y present to decay below detection limits. Experimental pH was also determined on an Orion bench top meter using electrodes calibrated at 4, 7 and 10 before and after sediment addition and at each time point. In all tests the % ^{90}Sr sorption was calculated from activities of ^{90}Sr in solution as follows:

$$\%^{90}Sr_{sorb} = \frac{A_i - A_e}{A_i} \times 100 \quad (1)$$

Where A_i = initial added activity (Bq ml^{-1}), A_e = activity after sorption (Bq ml^{-1}).

Further the apparent distribution coefficient between solid and aqueous phase (K_d, L kg^{-1}) was calculated using the following equation [6].

$$K_d = \frac{A_i - A_e}{A_e} \times \frac{V}{W} \quad (2)$$

Where V is the solution volume (ml) and W is the weight of sediment (g).

Section S3: Detailed X-ray Absorption Spectroscopy Methods

EXAFS spectra were collected from sediment samples at the Dutch Belgian beamline station BM26A at the European Synchrotron Radiation Facility (ESRF) in January 2011. Sr K-edge (16, 105 eV) spectra were collected while operating at 6 GeV with a typical current of 190 mA, using a nitrogen cooled Si(111) double crystal monochromator and focussing optics. A pair of collimating mirrors was used to reduce the harmonic content of the beam and the beam size was approximately 0.1 x 3 mm at the sample. See [7] for further details of station set-up and protocols. Spectra were collected from sediment samples aged in young cement water solution for 10 or 365 days, and from a further sample that had been aged at 70 C° for 365 days. For analysis, approximately 300 mg moist sediment samples were prepared for XAS analysis under an argon atmosphere packed in aluminium or Teflon holders with Kapton™ tape windows. All sediment samples were transported to the ESRF at −78 °C using dry ice. All data were collected in fluorescence mode using a 9 element solid state Ge detector and 4 - 8 scans per sample. Sediment sample data were collected at 80 ^{o}K using an Oxford Instruments CCC 1204 liquid nitrogen cooled cryostat. Results were compared to data collected from an aqueous Sr^{2+} (3000 mg L^{-1} as $SrCl_2$) and $SrCO_3$ standards (collect in transmission mode) collected at room temperature, also held in a Teflon holder using Kapton™ tape windows. Multiple scans were averaged to improve the signal to noise ratio using Athena version 0.8.061 [8] and data were background subtracted for EXAFS analysis using PySpline v1.1 [9]. There was very little drift in the Sr absorption edge during data collection, therefore no adjustment of E_0 was required prior to EXAFS fitting.

EXAFS data were analysed in DLexcurv v1.0 [10] using full curved wave theory [11]. Phaseshifts were derived from *ab initio* calculations using Hedin-Lundqvist potentials and von-Barth ground states [12]. Fourier transforms of the EXAFS spectra were used to obtain an approximate radial distribution function around the central Sr atom (the absorber atom); the peaks of the Fourier transform can be related to “shells” of surrounding backscattering ions characterised by atom type, number of atoms, absorber-scatterer distance, and the Debye-Waller factor (± 25%), $2\sigma^2$. Atomic

distances calculated by DLexcurv have an error of approximately ± 0.02 Å in the first shell, and ± 0.05 Å in subsequent shells. The data were fitted for each sample by defining a theoretical model and comparing the calculated EXAFS spectrum with experimental data. Shells of backscatterers were added around the Sr and by refining an energy correction Ef (the Fermi Energy, delta E; which for final fits typically varied between -5.2 and -1.6), the absorber-scatterer distance, and the Debye-Waller factor for each shell, a least squares residual (the *R* factor [13] was minimised. The amplitude factor (or AFAC in DLexcurv V1.0) was retained as the default of 1 throughout. Shells or groups of shells were only included if the overall fit (*R*-factor) was reduced overall by >5%. For shells of backscatterers around the central Sr, the number of atoms in the shell was chosen as an integer to give the best fit and then further refined.

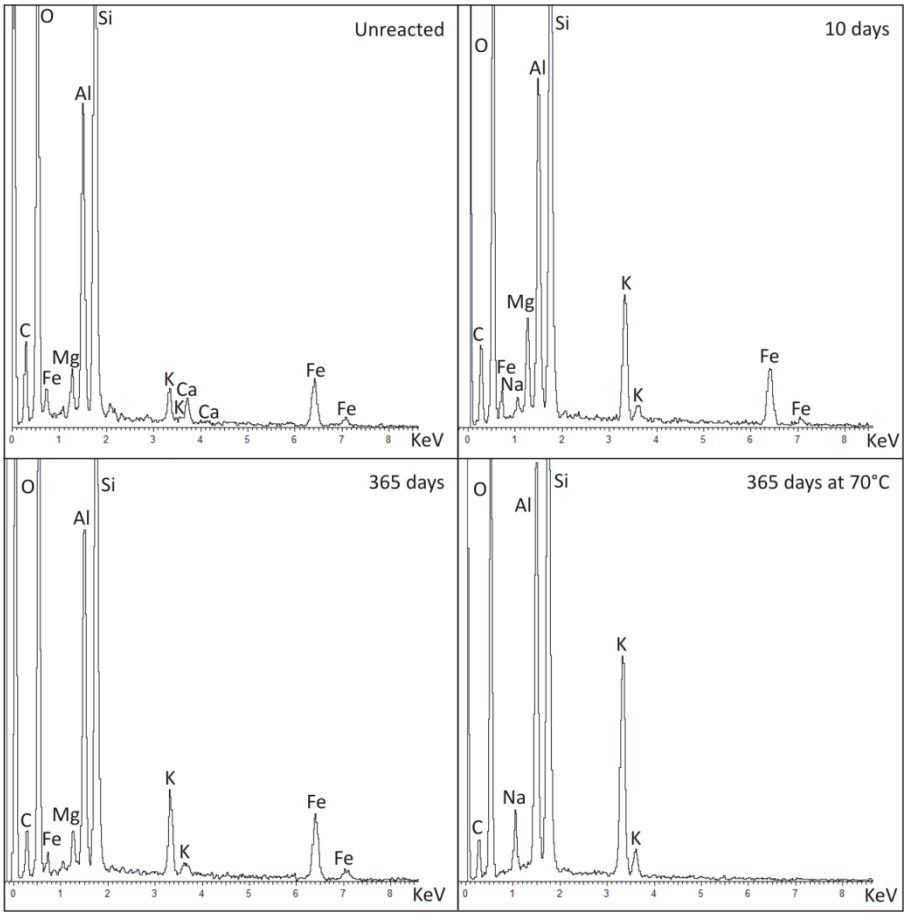

Figure S1. Spot analysis SEM-EDX spectra collected from sediment particle coatings before and after reaction with YCW for 10, 365 and 365 days +70^{o}C.

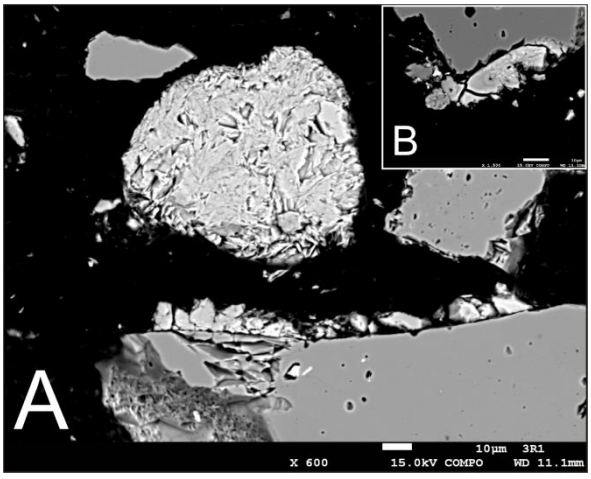

Figure S2. A) Electron microprobe image of neoformed chabazite crystals (appears brighter in image) in sediments after reaction with YCW for 365 days at 70 ^{o}C. A & B) Chabazite crystals commonly occur as coatings on the edge of larger quartz grains (appear grey in images).

Table S2. Microprobe raw data, oxide wt %

Target	SiO_2	Al_2O_3	MgO	CaO	Na_2O	K_2O	SrO	BaO	Total
1	34.469	27.351	0.144	2.378	3.510	7.444	2.582	0.081	77.959
2	35.856	23.020	0.152	1.696	2.330	10.367	2.614	0.048	76.083
3	44.481	19.831	0.431	0.531	1.161	10.967	0.389	0.172	77.962
4	40.044	22.946	0.171	0.746	1.536	11.739	1.715	0.011	78.909
5	34.664	24.311	0.025	0.964	0.489	15.250	3.974	0.002	79.678
6	40.520	23.271	0.442	3.300	2.140	8.249	1.772	0.046	79.740
7	41.089	22.271	0.407	2.284	0.844	10.573	1.180	0.068	78.717
Average	38.732	23.286	0.253	1.700	1.716	10.655	2.032	0.061	78.435

Table S3. Microprobe data – chemical formula calculations

Oxide	Av Wt %	Mol wt	Mol prop	Cat^+ prop	No. of O	No. of Cat^+
SiO_2	38.732	60.084	0.645	0.645	1.289	3.562
Al_2O_3	23.286	101.961	0.228	0.457	0.685	2.524
MgO	0.253	40.304	0.006	0.006	0.006	0.035
CaO	1.700	56.077	0.030	0.030	0.030	0.167
Na_2O	1.716	61.979	0.028	0.055	0.028	0.306
K_2O	10.655	94.196	0.113	0.226	0.113	1.250
SrO	2.032	103.619	0.020	0.020	0.020	0.108
BaO	0.0611	153.329	0.0004	0.0004	0.0004	0.002
Total	78.435				2.172	

Oxygen factor = 12/2.172 = 5.525

100 – Av Wt% = 21.565 and was assumed to be due to structural H_2O.

Calculated formula = $(K_{1.2},Na_{0.3}, Sr_{0.1},Ca_{0.1})$ $[Al_{2.5}Si_{3.6}O_{12}].5.9\ H_2O$

Table S4. Solution compositions used for PHREEQC geochemical modelling; based on the elemental analysis of experimental solutions after 365 days incubation of sediments and YCW at 21 ^{o}C. pH = 13.5.

Elements	Molality	Moles
Al	1.57E-03	1.57E-03
K	2.40E-01	2.40E-01
Na	7.37E-02	7.37E-02
Si	7.71E-04	7.71E-04

Table S5. Mineral saturation indexes calculated using the water composition determined after incubation of sediments in YCW for 365 days (SI Table S4). Results based on PHREEQC modelling using the Laurence Livermore National Laboratory (LLNL) database.

	Phase	SI	Log IAP	Log KT
Albite	NaAlSi3O8	-7.8	-5.14	2.66
Albite_high	NaAlSi3O8	-9.12	-5.14	3.98
Albite_low	NaAlSi3O8	-7.8	-5.14	2.66
Analcime	Na.96Al.96Si2.04O6:H2O	-4.35	1.71	6.06
Analcime-dehy	Na.96Al.96Si2.04O6	-10.71	1.72	12.42
Andalusite	Al2SiO5	-10.95	4.93	15.88
Beidellite-H	H.33Al2.33Si3.67O10(OH)2	-18.59	-14.1	4.49
Beidellite-K	K.33Al2.33Si3.67O10(OH)2	-15.08	-9.92	5.16
Beidellite-Na	Na.33Al2.33Si3.67O10(OH)2	-15.58	-10.08	5.5
Boehmite	AlO2H	-1.13	6.42	7.55
Chalcedony	SiO2	-4.16	-7.92	-3.76
Coesite	SiO2	-4.7	-7.92	-3.22
Corundum	Al2O3	-5.44	12.85	18.29
Cristobalite(alpha)	SiO2	-4.44	-7.92	-3.48
Cristobalite(beta)	SiO2	-4.89	-7.92	-3.03
Diaspore	AlHO2	-0.72	6.42	7.15
Gibbsite	Al(OH)3	-1.32	6.42	7.74
Jadeite	NaAl(SiO3)2	-5.53	2.78	8.31
K-Chabazite	K2Al2Si4O12:6H2O	**107.57**	6.47	-101.1
K-Feldspar	KAlSi3O8	-4.29	-4.67	-0.38
K2O	K2O	-58.7	25.34	84.04
Kalsilite	KAlSiO4	0.32	11.17	10.85
Kaolinite	Al2Si2O5(OH)4	-9.72	-3	6.72
Kyanite	Al2SiO5	-10.68	4.93	15.61
Leucite	KAlSi2O6	**8.77**	3.25	-5.52
Maximum_Microcline	KAlSi3O8	-4.29	-4.67	-0.38
Muscovite	KAl3Si3O10(OH)2	-5.27	8.18	13.45
Na2O	Na2O	-43.04	24.38	67.42
Na2SiO3	Na2SiO3	-5.74	16.46	22.2
Na4SiO4	Na4SiO4	-29.75	40.84	70.6
Na6Si2O7	Na6Si2O7	-44.23	57.3	101.53
Natrolite	Na2Al2Si3O10:2H2O	-4.93	13.46	18.39
Natrosilite	Na2Si2O5	-9.52	8.54	18.07
Nepheline	NaAlSiO4	-3.05	10.7	13.75
Paragonite	NaAl3Si3O10(OH)2	-9.68	7.7	17.38
Pyrophyllite	Al2Si4O10(OH)2	-19.12	-18.83	0.29
Quartz	SiO2	-3.89	-7.92	-4.03
Sanidine_high	KAlSi3O8	-5.48	-4.67	0.82
Sillimanite	Al2SiO5	-11.31	4.93	16.24
SiO2(am)	SiO2	-5.18	-7.92	-2.74

SI References List

1. Clausen, L.; Fabricius, I., BET Measurements: Outgassing of Minerals. *Journal of Colloid and Interface Science* **2000,** *227*, (1), 7-15.
2. Tessier, A.; Campbell, P. G. C.; Bisson, M., Sequential extraction procedure for the speciation of particulate trace metals. *Anal. Chem.* **1979,** *51*, (7), 844-851.
3. Kersten, M.; Förstner, U., Effect of sample pretreatment on the reliability of solid speciation data of heavy metals - implications for the study of early diagenetic processes. *Mar. Chem.* **1987,** *22*, (299-312).
4. Wallmann, K.; Kersten, M.; Gruber, J.; Förstner, U., Artifacts in the determination of trace metal binding forms in anoxic sediments by sequential extraction. *Intern. J. Environ. Anal. Chem.* **1993,** *51*, 187-200.
5. Wallace, S. H.; Shaw, S.; Morris, K.; Small, J. S.; Fuller, A. J.; Burke, I. T., Effect of groundwater pH and ionic strength on strontium sorption in aquifer sediments: Implications for 90Sr mobility at contaminated nuclear sites. *Applied Geochemistry* **2012,** *27*, (8), 1482-1491.
6. Khan, S. A.; Riaz ur, R.; Khan, M. A., Sorption of strontium on bentonite. *Waste Management* **1995,** *15*, (8), 641-650.
7. Nikitenko, S.; Beale, A. M.; van der Eerden, A. M. J.; Jacques, S. D. M.; Leynaud, O.; O'Brien, M. G.; Detollenaere, D.; Kaptein, R.; Weckhuysen, B. M.; Bras, W., Implementation of a combined SAXS/WAXS/QEXAFS set-up for time-resolved in situ experiments. *Journal of Synchrotron Radiation* **2008,** *15*, 632-640.
8. Ravel, B.; Newville, M., ATHENA, ARTEMIS, HEPHAESTUS: data analysis for X-ray absorption spectroscopy using IFEFFIT. *Journal of Synchrotron Radiation* **2005,** *12*, 537-541.
9. Tenderholt, A.; Hedman, B.; Hodgson, K. O., PySpline: A modern, cross-platform program for the processing of raw averaged XAS edge and EXAFS data. In *X-Ray Absorption Fine Structure-XAFS13*, Hedman, B. P. P., Ed. 2007; Vol. 882, pp 105-107.
10. Tomic, S.; Searle, B. G.; Wander, A.; Harrison, N. M.; Dent, A. J.; Mosselmans, J. F. W.; Inglesfield, J. E. *New Tools for the Analysis of EXAFS: The DL_EXCURV Package, CCLRC Technical Report DL-TR-2005-00, ISSN 1362-0207*; Daresbury SRS 2005: 2005.
11. Gurman, S. J.; Binsted, N.; Ross, I., A RAPID, EXACT CURVED-WAVE THEORY FOR EXAFS CALCULATIONS. *Journal of Physics C-Solid State Physics* **1984,** *17*, (1), 143-151.
12. Binsted, N. *EXCURV98: CLRC Daresbury Laboratory computer program*, CLRC Daresbury, Warrington, UK., 1998.
13. Binsted, N.; Strange, R. W.; Hasnain, S. S., CONSTRAINED AND RESTRAINED REFINEMENT IN EXAFS DATA-ANALYSIS WITH CURVED WAVE THEORY. *Japanese Journal of Applied Physics Part 1-Regular Papers Short Notes & Review Papers* **1993,** *32*, 141-143.